Calculation of state selective field ionization of hydrogen atoms in a strong magnetic field

2011 J. Phys. B: At. Mol. Opt. Phys. 44 184003

(http://iopscience.iop.org/0953-4075/44/18/184003)

J. Phys. B: At. Mol. Opt. Phys. **44** (2011) 184003 (8pp) doi:10.1088/0953-4075/44/18/184003

Calculation of state selective field ionization of hydrogen atoms in a strong magnetic field

P H Donnan, K Niffenegger, T Topcu and F Robicheaux

Department of Physics, Auburn University, AL 36849-5311, USA

E-mail: robicfj@auburn.edu

Received 17 February 2011, in final form 22 March 2011
Published 14 September 2011
Online at stacks.iop.org/JPhysB/44/184003

Abstract

We have performed classical and quantum calculations for a hydrogen atom in a strong magnetic field exposed to a parallel electric field that linearly increases with time. The calculations were performed for the situation where the electron is launched from near the nucleus and for a microcanonical ensemble. For the case of low angular momentum, the classical and quantum calculations are compared. We show that there exist stable classical trajectories at positive energy and that these contribute to the possibility of the atom surviving to strong electric fields. The dependence of the survival probability versus electric field strength can be used to estimate the behaviour of Rydberg anti-hydrogen atoms in the ALPHA and ATRAP experiments.

1. Introduction

State selective field ionization (SSFI) [1] uses an electric field that increases with time to destructively measure the character of the Rydberg state of an atom or molecule. At the simplest level, there is a correspondence between binding energy and the electric field at which the electron leaves the atom with the more weakly bound states being ionized at weaker fields. This correspondence occurs for low angular momentum states in atoms because most of the crossings are adiabatic as the energy levels fan out under the influence of the electric field. Thus, the energy of the state does not strongly change with electric field strength and it ionizes when the energy of the state is above the classical ionization threshold. This leads to the approximate relation for the field to strip the electron from the atom: $F_{\rm strip} \sim 5.14 \times 10^9$ V cm$^{-1}/(16n^4)$ where 5.14×10^9 V cm^{-1} is the atomic unit of the electric field and n is the principal quantum number of the state. For low angular momentum states in atoms, the actual stripping field is somewhat higher than this simple estimate because the energy of the atom trends to somewhat lower values as the electric field increases.

The hydrogen atom and states with large L_z do not behave in this simple manner because the $1/r$ potential plus electric field separates in parabolic coordinates. As long as the electric field is changing slowly compared to the Rydberg period, the energy levels cross and the field needed to strip the atom depends on the binding energy *and* the electric dipole moment. States where the energy decreases with electric field strength are stripped at much lower fields than states where the energy increases with electric field strength. Not only are states with energies higher than the classical ionization threshold essentially stable, there are even states with total positive energy that are essentially stable. In the classical system, there are stable islands at positive energy.

The presence of a magnetic field could qualitatively change this behaviour. Vrinceanu *et al* [2] performed calculations of SSFI for a hydrogen atom in a strong magnetic field. In this study, they mainly focused on guiding centre type of atoms where the size of the atom is large compared to the cyclotron orbit of the electron (e.g. see [4]). They were also interested in how the motion of the atom across the magnetic field affected the dynamics. Choi *et al* [3] performed measurements of SSFI in Rb Rydberg states in magnetic fields up to 6 T. They could clearly see the different thresholds formed by different number of quanta in the electron's cyclotron motion (Landau levels).

The study of SSFI for hydrogen in a strong magnetic field has both an intrinsic interest and is also important for the recent experiments that have trapped the antimatter version of the hydrogen atom [5]. This system is intrinsically interesting because both the $B = 0$ and the $B \to \infty$ limits are relatively

simple to understand. However, several interesting questions arise when the magnetic field is strong enough to perturb the system but not so strong as to dominate. It is known that the classical system of a hydrogen atom in parallel electric and magnetic fields is chaotic. Does the magnetic field cause a coupling between the states so that the SSFI spectrum is more like an alkali atom in a low angular momentum state (that is, are the level crossings adiabatic) or does there exist stable regions of phase space so that states above the classical ionization threshold, or even at positive energies, are stable (that is, are the level crossings diabatic)? Another possible question is whether classical calculations can give a decent representation of quantum calculations. The importance of the antihydrogen experiments is that the antihydrogen atoms are made in a strong magnetic field (approximately 1 T) but travel through regions of small and large electric fields. Thus, it is important to know at what electric field strength the positron is stripped from the antiproton for strong magnetic fields.

The SSFI of a hydrogen atom in a parallel magnetic field is a continuation of a long series of studies of parallel electric and magnetic fields extending over decades. Except for [2, 3], these studies have been for the case where the electric and magnetic fields are constant. Several studies have been for somewhat weak fields so that perturbative quantum treatments are useful [6–8]. There have been several theoretical quantum studies of hydrogen and alkali atoms using advanced numerical techniques to accurately compute properties of this system [9–15]. Several classical studies of atoms in parallel electric and magnetic fields have contributed to the understanding of the complicated dynamics [16–18]. Finally, there have been semiclassical studies that have focussed on the effect of closed classical orbits [19–21].

In this paper, we study the SSFI for a hydrogen atom in a strong magnetic field but for more deeply bound states than those investigated in [2, 3]. In the first part of the paper, we perform calculations for states with low canonical angular momentum for five different magnetic field strengths (0, 1, 2, 4, 8 T), several different ramp rates and for two different initial binding energies. For these calculations, we compare the results from quantum and classical calculations. The idea behind these calculations is to show how the SSFI spectra vary as the magnetic field is increased and to qualitatively understand trends in the data. In the second part of the paper, we calculate the SSFI spectrum for a microcanonical ensemble. These results could be useful for the antihydrogen experiments because [22] showed that positron collisions with antihydrogen caused the bound positron distribution to only be a function of the binding energy with all other variables populated ergodically; thus, the distribution can be thought of as an integral over microcanonical ensembles with the energy distribution depending on temperature, density, etc. In the last part of the paper, we examine the classical phase space for trajectories at positive energies and show that there are classically stable islands.

2. Numerical method

We solved both the classical and quantum time-dependent equations for the parallel electric and magnetic fields. Some of the details are given in the next two sections.

In all of the calculations, the nucleus is taken to be infinitely massive and fixed in space. We can make this approximation because the cases we are interested in are for relatively deeply bound states and for atoms that have a low speed. When the atom is slow, transformations can be made to the Hamiltonian (see for example, equation (6) of [2]) that give an effective electric field perpendicular to the magnetic field with a strength of $v_\perp B$ where $v_\perp$ is the atom's velocity perpendicular to B. For the antimatter experiments, $v_\perp$ is of order 100 m s^{-1} and B is of order 1 T. This gives an effective electric field of order 100 V m^{-1} = 1 V cm^{-1}. As will be seen in section 3, this is a weak electric field for the cases we study.

2.1. Classical calculations

We solved the full classical equations of motion using an adaptive step-size Runge–Kutta algorithm [23]. The equations of motion are

$$\frac{\mathrm{d}\vec{r}}{\mathrm{d}t} = \vec{v}$$
$$\frac{\mathrm{d}\vec{v}}{\mathrm{d}t} = -\frac{q^2\vec{r}}{4\pi\varepsilon_0 m r^3} + q(F(t)\hat{z} + \vec{v}\times(B\hat{z}))/m \qquad (1)$$

where $q = -1.602\times10^{-19}$ C is the charge of an electron and $m = 9.109\times10^{-31}$ kg is the mass of an electron. We have chosen the z-direction to be the direction of the electric and magnetic fields. Because the Runge–Kutta algorithm is not symplectic, there is some worry that the results will be affected by numerical drag. This is especially true since the classical equations of motion are chaotic when the magnetic field is non-zero. We have controlled this effect in two ways. The first is to monitor the conserved quantities. If the electric field is held fixed, then the energy and the canonical angular momentum about the z-axis are conserved; if the electric field is changing then only the canonical angular momentum about the z-axis is conserved. During every run, we monitored the accuracy with which the conserved variables remain unchanged. Any run that gave too large a change in a conserved quantity was rejected. For the results below, less than 0.2% of the runs were rejected. The second method is to repeat the calculation with the accuracy condition increased by a factor of 10 until successive SSFI spectra agreed.

Another worry is that the electric field should smoothly turn on to avoid artifacts from discontinuities in the time derivative of the Hamiltonian. To avoid this we chose the time-dependent electric field to have the form

$$F(t) = t_{\mathrm{wid}}\frac{F_{\mathrm{max}}}{t_{\mathrm{fin}}}\ln(1+\mathrm{e}^{t/t_{\mathrm{wid}}}) \qquad (2)$$

where t_{wid} gives the effective time width over which the field ramps on and where F_{max} is the maximum electric field which is achieved at the final time of the simulation, t_{fin}. This functional form has the property that it smoothly increases from 0 as t approaches 0 from below and then smoothly

becomes a linear function of time when t is larger than $t_{\rm wid}$. To see the different asymptotic behaviours, note that

$$F(t) \simeq t_{\rm wid}\frac{F_{\rm max}}{t_{\rm fin}}\,{\rm e}^{t/t_{\rm wid}} \qquad \text{for} \quad t < -3t_{\rm wid}$$
$$F(t) \simeq \frac{F_{\rm max}}{t_{\rm fin}}(t + {\rm e}^{-t/t_{\rm wid}}) \qquad \text{for} \quad t > 3t_{\rm wid}. \tag{3}$$

Typically, we chose $t_{\rm wid}$ to be 0.5% of the total time of the simulation, $t_{\rm fin}$. The starting time was always chosen to be before $-0.07t_{\rm fin}$; thus, the initial $t/t_{\rm wid}$ was always less than -14 which gives a field at the starting time less than $F_{\rm max}\,{\rm e}^{-14}/200 \simeq 4.2\times10^{-9}F_{\rm max}$.

2.2. Quantum calculations

We solved for the quantum wavefunction using an expansion in radial functions with spherical harmonics:

$$\Psi(\vec{r},t) = \sum_{\ell} G_\ell(r,t)Y_{\ell m}(\theta,\phi) \tag{4}$$

with the radial functions $G_\ell(r,t)$ being represented on a grid of radial points using a square root mesh [24]. We solved the time–dependent Schrodinger equation using a split operator method:

$${\rm e}^{-{\rm i}H\delta t/\hbar} \rightarrow {\rm e}^{-{\rm i}H_2\delta t/(2\hbar)}\,{\rm e}^{-{\rm i}H_1\delta t/\hbar}\,{\rm e}^{-{\rm i}H_2\delta t/(2\hbar)}. \tag{5}$$

The splitting was such that H_1 was the atomic Hamiltonian with no field and H_2 was the Hamiltonian from the electric field and the Zeeman and diamagnetic magnetic field terms. The H_1 is diagonal in ℓ but couples together neighbouring radial points. The H_2 is diagonal in r but is penta-diagonal in ℓ because the electric field couples ℓ to $\ell\pm1$ and the diamagnetic term couples ℓ to $\ell\pm2$. One of the advantages of the split operator method is that the propagator is exactly unitary so that the norm of the wavefunction is constant.

We approximated each of the exponential propagators using an implicit method:

$${\rm e}^{-{\rm i}H_1\delta t/\hbar} \rightarrow [1-{\rm i}H_1\delta t/(2\hbar)]/[1+{\rm i}H_1\delta t/(2\hbar)]. \tag{6}$$

The implicit method has several advantages over all other methods when propagating highly excited states of atoms. The two most important are that the propagator is exactly unitary so that the norm of the wavefunction stays constant *and* the time step δt can be chosen to be commensurate with the physics instead of being determined by irrelevant quantities (like the size of the radial steps).

Both approximations have an error during one time step of order δt^3; this will give a cumulative error of order δt^2. We decreased the size of δt by factors of 2 until the SSFI spectra were converged.

Another source of error is in the expansion of the wavefunction in a basis of $Y_{\ell m}$. We made sure that the calculation was converged with respect to the largest angular momentum by changing the maximum number of angular momenta with time. After each time step, we computed the probability for finding the electron in each ℓ by integrating the $|G_\ell(r,t)|^2$ with respect to r. We then had the maximum ℓ set to be 10 plus the largest ℓ that had a probability of at least 10^{-10}.

A final source of error is the number of radial points. We used a Numerov-like expression for the kinetic energy [25]. We increased the number of radial points until convergence of the SSFI signal was achieved. In the calculation below, we used a radial region out to $r = 5000a_0$ with 2000 points for the $n = 30$ calculations.

Computing the SSFI spectrum requires the escape of the electron to be treated properly. In our calculations, we obtained the same results whether we used a complex absorbing potential or a radial mask. For the calculations below, the mask or complex absorbing potential was gradually turned on from $r = 3500a_0$ for the $n = 30$ calculations. This gives a range of $1500a_0$ over which the outgoing probability is absorbed. For calculations at different n, all of the distances were scaled by a factor of n^2 and the number of points was scaled by n. Some care needs to be taken with the mask or absorbing potential because if the absorption is too weak the electron will reach the edge of the radial range and reflect from the hard wall back into the region near the atom. Also, if the absorption is turned on too quickly, the electron can reflect from the mask or complex potential. To ensure that reflection was not contaminating our results, we varied the absorption strength by factors of 2 until the plots of the wavefunction showed no reflection and the SSFI spectrum was converged.

3. Results

3.1. Low angular momentum case

We performed classical and quantum calculations where the electron is launched from the nucleus, radially outward, and after a short delay the electric field is ramped. This situation will give a canonical angular momentum about the z-axis to be 0. This case was of interest to us because it involves the possibility of the electron passing close to the nucleus.

For all of the calculations, the asymptotic ramp rate in equation (2) is

$$\frac{{\rm d}F}{{\rm d}t} = \frac{F_{\rm max}}{t_{\rm fin}} \tag{7}$$

where $F_{\rm max}$ was the maximum electric field which was achieved at the final time of the simulation, $t_{\rm fin}$. In the calculations below, we varied the final time, $t_{\rm fin}$, in order to illustrate the role of the ramp rate. We also fixed the width of the turn on of the electric field in equation (2) to be

$$t_{\rm wid} = \frac{t_{\rm fin}}{200}. \tag{8}$$

The quantum mechanical way to launch an $\ell = 0$ wave packet is to solve the inhomogeneous Schrodinger equation:

$${\rm i}\frac{\partial\Psi}{\partial t} - H\Psi = S(r)\,{\rm e}^{-{\rm i}E_0t/\hbar}\,{\rm e}^{-[(t-t_0)/\Delta t]^2} \tag{9}$$

where $S(r)$ is only a function of r and is non-zero for a small region of r (less than $5a_0$), E_0 is the central energy of the wave packet, t_0 is the time at which the wave packet is launched and Δt is the width in time of the launch. In all calculations of this section, the width Δt was taken to be 1/4 of a Rydberg period at energy E. The time of the launch was taken to be

$t_0 = -0.07t_{\rm fin} - 6\Delta t$; this launch time insures that the electric field is essentially 0 during the whole launch.

By taking the duration of the launch to be 1/4 of the Rydberg period, the energy width of the packet is approximately the spacing of the zero field Rydberg levels. This means that states with n and $n \pm 1$ are the main states excited. The reason for wanting to limit the launch width to less than a period means the electron wave does not have time to reflect from the large r potential and return to the region near the nucleus, setting up a standing wave.

To most closely match the quantum calculation, the classical calculation should have specific initial conditions. In the classical calculation, we launch the electron at a small distance from the nucleus (1 a_0) with a velocity in the radial direction. The launch time is chosen randomly with a distribution proportional to

$$P_t(t) \propto \mathrm{e}^{-2[(t-t_0)/\Delta t]^2} \tag{10}$$

because the right-hand side of equation (9) gives the *amplitude* to launch as a function of time. The energy of the electron at the launch is chosen randomly from a distribution proportional to

$$P_E(E) \propto \mathrm{e}^{-[(E-E_0)\Delta t/\hbar]^2/2} \tag{11}$$

which correctly matches the energy distribution of the quantum wave packet.

3.1.1. $n = 30$. We performed calculations for a central energy, E_0, corresponding to field-free $n = 30$ states. An important point of comparison for the figures below is the estimate of the field strength of ionization using an adiabatic evolution of energy: $F_{\rm strip} \sim 5.14 \times 10^9\ \mathrm{V\ cm^{-1}}/(16n^4) \simeq 400\ \mathrm{V\ cm^{-1}}$. In all of the calculations, we set the maximum field strength to be 6000 V cm^{-1} which is over an order of magnitude larger than the nominal stripping field of 400 V cm^{-1}; as will be seen in the figures below, this large a field strength is needed in some cases.

In figure 1, we show the classical survival probability versus field strength for a 4 T magnetic field and for different final times. This comparison gives an idea about how slowly an electric field needs to be ramped before the results become similar. The upper part of figure 1 shows the classical survival probability when the final time is 0.2 ns, 0.8 ns and 3.2 ns; for this sequence the ramp rate is getting slower by a factor of 4 between each curve. From this figure, it is clear that there is little change in the classical survival as a function of field strength once the ramp rate has sufficiently slowed. We found that lower magnetic field strengths tended to give similar survival probabilities for faster ramp rates.

The trend is that the faster ramp rates (i.e. smaller final time) have a survival probability that extends to larger electric fields. There are two effects that contribute to this trend. The first is because the size of the stable phase space is shrinking as the electric field increases. However, in the unstable region of phase space that is near the stable region, it can take the electron a substantial amount of time to find the hole in phase space to leave the atom. If the electric field is ramped quickly, the electron will leave the atom after the electric field has increased from the value where it could have decayed. The second effect is that the magnetic field can add other relevant time scales to the system so that the rapidity of the ramp can cause the electron to transfer energy between different types of motion.

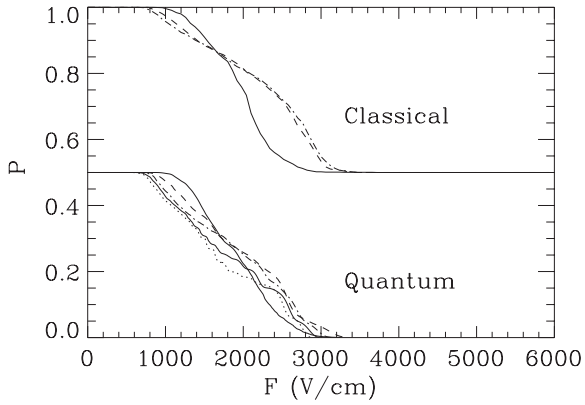

Figure 1. The classical (upper half of the plot) and quantum (lower half of the plot) survival probability as a function of electric field strength for electrons launched with energy corresponding to $n = 30$. The magnetic field is 4 T. The final electric field is 6000 V cm^{-1} and the final time is 0.2 ns (solid line), 0.8 ns (dashed line), 3.2 ns (dash–dotted line), 12.8 (dash-dot-dot-dot line) and 51.2 ns (dotted line). The classical calculation only has the three shorter final times.

Quantum mechanics adds other time dependences that need to be checked. Figure 1 shows the quantum survival probability when the final time is 0.2 ns, 0.8 ns, 3.2 ns, 12.8 ns and 51.2 ns. Although the qualitative behaviour does not change for times longer than 3.2 ns, there are larger differences than in the classical calculation. There are two other kinds of processes which can lead to differences for different ramp rates. The first is due to the fact that the wavefunction can tunnel from stable regions into unstable regions; when the ramp rate is high, the effect from this tunnelling will be less. The second is that there are quantum interferences that arise from the partially adiabatic/diabatic crossings of energy levels. As the ramp rate changes, the amount of phase accumulated through different paths will change which will lead to interference that changes with the ramp rate.

In figure 2, we show the SSFI spectrum for different magnetic field strengths. The SSFI spectrum is proportional to -1 times the derivative of the survival probability. This figure shows the classical spectrum for a final time of 12.8 ns. The SSFI spectra for longer final times do not qualitatively differ from those plotted. The most obvious trend is that the SSFI spectrum tends to get broader and shift to higher electric field strengths with increasing magnetic field, but with two important exceptions. The first exception is that the SSFI spectrum at 1 T is somewhat narrower than the 0 T spectrum; this seems to be mostly due to a slight delay in the onset of ionization but also partially due to less trajectories being stable at higher electric fields. The other interesting exception is the 8 T case where the ionization starts at electric fields of approximately 370 V cm^{-1}. This onset is earlier by $\sim$300 V cm^{-1} than the 0 T case and is near the value expected

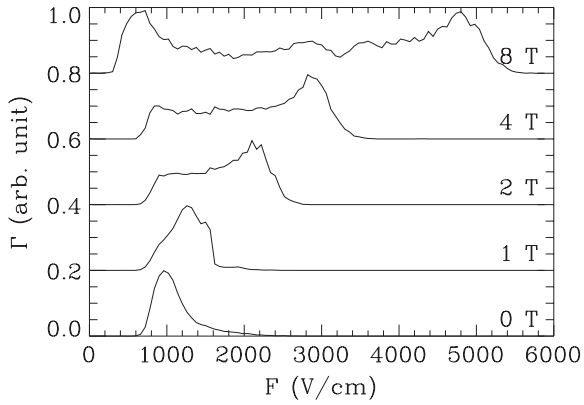

Figure 2. The classical SSFI spectrum for (from lowest to highest) $B = 0$ T, 1 T, 2 T, 4 T and 8 T for electrons launched with energy corresponding to $n = 30$. These results are for a final time of 12.8 ns. The SSFI spectrum is proportional to the negative of the derivative of the survival probability. As the magnetic field increases, the SSFI spectrum is spread over a larger range of electric field.

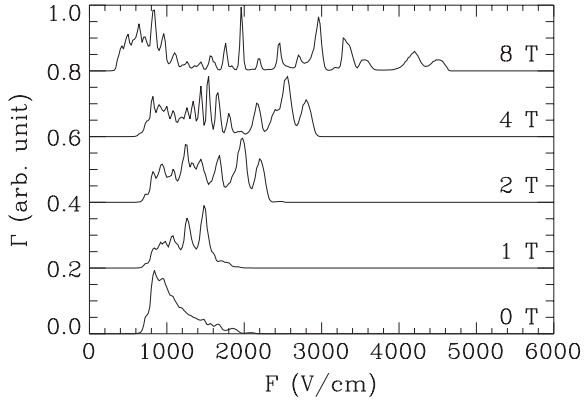

Figure 3. The quantum SSFI spectrum for (from lowest to highest) $B = 0$ T, 1 T, 2 T, 4 T and 8 T for electrons launched with energy corresponding to $n = 30$. These results are for a final time of 25.6 ns. Compare to the classical result in figure 2.

from the simple estimate of 400 V cm^{-1}; however, the 8 T spectrum *is* the broadest spectrum. For the 8 T case, there is substantial SSFI spectrum out to ∼5000 V cm^{-1} which is over an order of magnitude larger than the simple estimate.

In figure 3, we show the quantum SSFI spectrum for different magnetic field strengths. The SSFI spectrum has been convolved with a $1/e$ half-width of 20 V cm^{-1}. The reason for the convolution is that the quantum SSFI signal consists of more than 100 narrow peaks with strongly varying heights and widths due to the spread of the population over more than 100 quantum states; the convolution is necessary to see the general features of the SSFI signal. This figure shows the spectrum for a final time of 25.6 ns so that some of the more finely detailed features are more apparent. The classical and quantum calculations show the same kind of general trends with magnetic field strength. For example, even the relatively early onset of the SSFI spectrum for the 8 T case is seen in the quantum calculation. The one glaring difference with the classical calculation is that the SSFI spectrum for $B \neq 0$ is

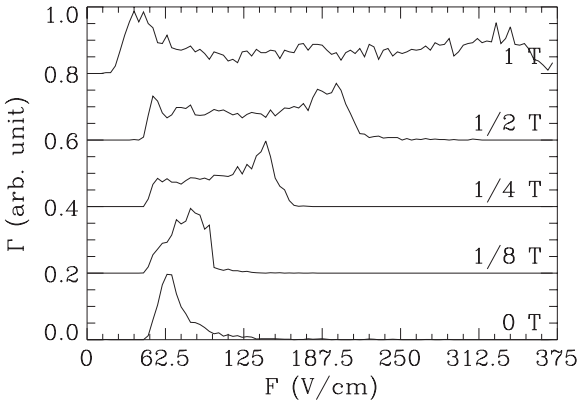

Figure 4. Same as in figure 2 but for (from lowest to highest) $B = 0$ T, 1/8 T, 1/4 T, 1/2 T and 1 T for electrons launched with energy corresponding to $n = 60$. These results are for a final time of 102.4 ns.

not smooth but consists of a series of peaks. The peaks do not line up with any simple trend that we tested. For example, in [3], they could experimentally see the different thresholds corresponding to different quanta in the cyclotron motion. For figure 3, the peaks for the 8 T case most nearly match a spacing of $2\hbar\omega_c$ (with $\omega_c = eB/m$ being the cyclotron angular frequency) but the agreement is not great. Perhaps the peaks more nearly match the initial excitation of discrete quantum states; because the different states have to be at approximately the same total energy, they have quite different character and ionize at different field strengths.

3.1.2. $n = 60$. We performed calculations for a central energy, E_0, corresponding to field free $n = 60$ states. An important point of comparison for the figures below is the estimate of the field strength of ionization using an adiabatic evolution of energy: $F_{\text{strip}} \sim 5.14 \times 10^9\,\text{V cm}^{-1}/(16n^4) \simeq 25$ V cm^{-1}. In all of the calculations, we set the maximum field strength to be 375 V cm^{-1} which is over an order of magnitude larger than the nominal stripping field of 25 V cm^{-1}. The classical calculation of a trajectory should exactly scale although we did not put the scaling into the equations of motion. This means classical results should be the same as for $n = 30$ if the electric field is scaled down by a factor of 16, the magnetic field is scaled down by a factor of 8 and the time is scaled up by a factor of 8. However, the initial conditions we have chosen mean that the energy width, $\Delta E \propto 1/\Delta t$, is a factor of 8 smaller than for $n = 30$ instead of the factor of 4 needed for perfect scaling, but this effect should not be large. Figure 4 shows the classical calculation similar to that in figure 2 but with all of the fields and times scaled. It is clear from the comparison that the features are similar except for the statistical noise.

The quantum calculations for a final time of 102.4 ns are shown in figure 5. The SSFI spectrum has been convolved with a $1/e$ half width of (20/16) V cm^{-1}. A comparison with figure 3 shows that the range of electric fields where the atom is stripped is roughly the same. However, the $n = 60$ results in figure 5 do not show as many peaks as seen for the $n = 30$

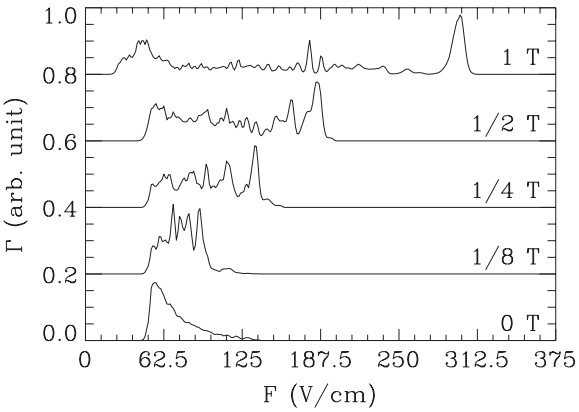

Figure 5. Same as in figure 3 but for (from lowest to highest) $B = 0$ T, 1/8 T, 1/4 T, 1/2 T and 1 T for electrons launched with energy corresponding to $n = 60$. These results are for a final time of 102.4 ns.

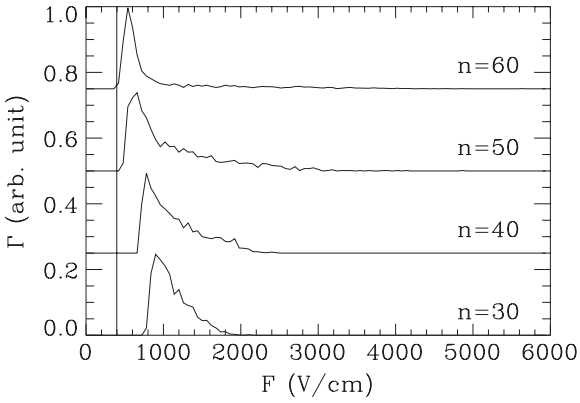

Figure 6. The classical SSFI spectrum for electrons with a microcanonical distribution for binding energies corresponding to (from lowest to highest) $n = 30$, 40, 50, and 60. All calculations are for $B = 1$ T. The electric field is scaled by the factor $(30/n)^4$ so all of the curves can be plotted on the same graph. The vertical line is the commonly used estimate of the stripping field: $F_{\text{strip}} \sim 5.14 \times 10^9$ V cm$^{-1}/(16n^4)$. The $n = 60$ calculation has the highest scaled magnetic field and gives electrons at the earliest time.

results. The reason is that there are more quantum states within the same scaled energy range for $n = 60$; as the quantum system becomes more nearly like the classical system, the SSFI spectrum should become more like the smooth classical spectrum.

3.2. Microcanonical ensemble

The recent calculations in [22] showed that the distribution of a positron attached to an anti-proton at a specified energy rapidly approaches the microcanonical ensemble when the atom is in a plasma. The nature of formation of anti-hydrogen in a positron plasma depends on the duration of the anti-proton in the positron plasma and the plasma parameters. Despite this, we expect that the distribution of states with an energy between $E - (\mathrm{d}E/2)$ and $E + (\mathrm{d}E/2)$ when the anti-hydrogen leaves the plasma will be more nearly like a microcanonical ensemble than like a distribution with a strongly biased angular momenta. Thus, it is worthwhile to calculate the SSFI spectrum for a microcanonical ensemble.

Figure 6 shows the classical SSFI spectrum for energies corresponding to $n = 30$, 40, 50 and 60; for all of the calculations the magnetic field was set to 1 T. The final time was taken to be long enough so that the spectrum no longer changed with the ramp rate. The SSFI field in each plot has been scaled by the factor of $(30/n)^4$. The vertical line marks the position of the simple estimate using $F_{\text{strip}} \sim 5.14 \times 10^9$ V cm$^{-1}/(16n^4)$. The SSFI spectrum is clearly changing with n even when plotted using a scaled x-axis. This is because the scaled magnetic field strength is changing with n. Because the magnetic field was held at 1 T, the effective field strength at $n = 60$ is a factor of 8 larger than for $n = 30$.

There are some clear features worth noting. First, the peak of the emission is at a field higher than the simple estimate. Second, the scaled peak moves closer to the simple estimate as the scaled magnetic field increases. For example, the peak for $n = 30$ is at a field approximately a factor of 2 larger than the simple estimate whereas the peak for $n = 60$ is at a field approximately a factor of 1.4 larger than the simple estimate. Third, the scaled width of the SSFI spectrum decreases as the scaled magnetic field increases. For example, the $n = 30$ spectrum has a substantial signal to 1400–1600 V cm^{-1} whereas the $n = 60$ spectrum only has a substantial signal to the scaled field of ~650 V cm^{-1}. Finally, the middle n has a small tail that extends to a very large field. For example, the $n = 50$ has a visible signal out to a scaled field of ~3000 V cm^{-1} whereas the $n = 30$ has no visible signal past ~2000 V cm^{-1}.

The fact that the SSFI spectrum peaks at a higher electric field means that an atom stripped at a specific electric field is less strongly bound than commonly estimated. The size of the shift depends on the relative size of the magnetic field. For the situation like that for the $n = 60$ plot in figure 6, the shift in binding energy is only ~20%. But for the situation like that for the $n = 30$ plot the shift in binding energy is ~40%. For some aspects of the atom, this is not a big change. However, there are properties (e.g. the time for a radiative cascade to reach the ground state) that would change by more than a factor of 2.

3.3. Stability of classical orbits

One question that might naturally arise is whether the classical orbits that survive to high fields would ionize if the electric field was ramped more slowly. Also, it would be interesting to know what kind of motion survives to high fields.

We first addressed these questions qualitatively. One feature that we found was that the quantum calculation corresponding to figures 3 and 5 gives a wavefunction which can be plotted as a function of time. We found that the wavefunction was strongly localized in the direction-up potential when the electric field reached the point where the bound state population had reached a smallish value (e.g. 20%). We found a similar type of behaviour for the classical trajectories when the classical bound state population reached a smallish value; the trajectories that survived were such that

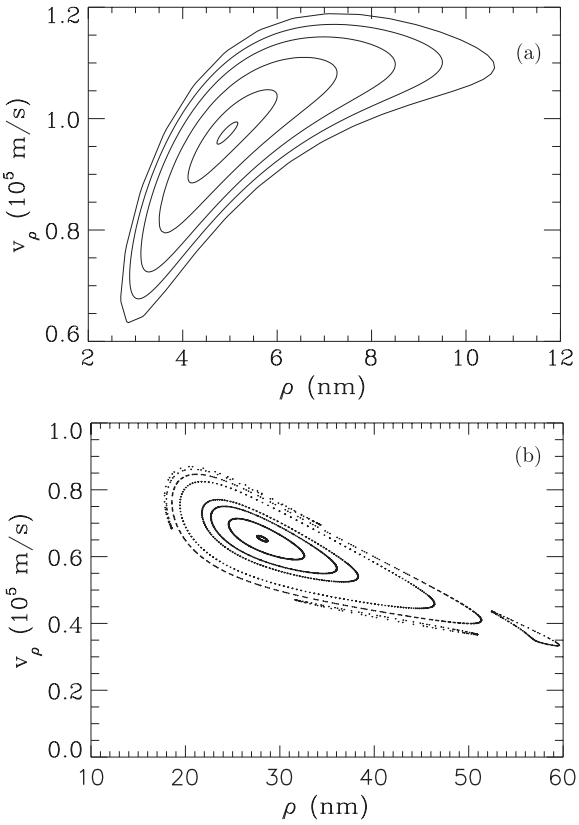

Figure 7. The Poincaré surface of section plot for $n = 30$ trajectories ramped to 2500 V cm^{-1} in a 4 T field. The plot in (a) corresponds to a higher energy but nearly zero angular momentum case. The plot in (b) corresponds to a somewhat lower energy (but still well above the classical ionization threshold) and a somewhat high angular momentum. See the text for details.

the electron's orbit mostly extended up the potential energy from the electric field. If we turned off the ramp so the electric field remained at a large constant value, we found that the classical trajectory survived for as long as we were willing to calculate which suggests that the classical orbits are stable. It was found in [18] that a stable classical orbit above the classical ionization threshold played a large role in the time-dependent ionization in a static electric and magnetic field. It appears that SSFI gives classically stable trajectories as well.

To more precisely check whether the classical orbit is stable, we used the Poincaré surface of section plot to visualize the motion. In the calculation, we ramped the electric field as before but then smoothly turned off the ramp so that the electric field went to a constant value. We then plotted $\rho = \sqrt{x^2 + y^2}$ and $v_\rho = (x v_x + y v_y)/\rho$ every time the trajectory goes through the plane $z = 100\ a_0$ with $v_z > 0$ for trajectories with the same E and canonical angular momentum about the z-axis. In figure 7 we show the Poincaré surface of section plot for two different cases. These plots clearly show closed surfaces which means that the trajectories inside of the outermost surface are stable. Both plots are for the case where we started the electron with an energy corresponding to $n = 30$ and ramped the electric field to the constant value 2500 V cm^{-1} in a magnetic field of 4 T. At this field, the classical ionization threshold is at an energy of -6.08×10^{-21} J. For figure 7(a), the canonical angular momentum around the z-axis was $-0.64\hbar$ and the energy was -2.72×10^{-22} J which is well above the classical ionization threshold. Since this trajectory has a small angular momentum, one can use the 4 T plot in figure 2 for orientation. For figure 7(b), the canonical angular momentum around the z-axis was $11.9\hbar$ and the energy was -1.78×10^{-21} J which is well above the classical ionization threshold.

4. Conclusions

We have performed classical and quantum calculations for the state selective field ionization of a hydrogen atom in a strong magnetic field. We found that the classical and quantum calculations agreed in their general features when the electron is launched from near the nucleus but the quantum calculations showed peaks which seem to be associated with specific states. Both the classical and quantum calculations have the SSFI spectrum peaking at larger fields than expected and the signal extending to much larger fields than expected. By inspecting the classical surface of section plots, we show that the classical orbits at high electric fields can be stable even when the total energy is positive.

We have also calculated the SSFI spectrum for microcanonical distribution of states. This distribution gives a single peak in the SSFI spectrum at higher field than from simple estimates. The relative shift is larger when the scaled magnetic field is smaller. This has implications for recent experiments leading to trapped anti-hydrogen. The delay in ionization means that atoms with smaller binding energy could survive the electric fields in the anti-matter traps. Since the main mechanism leading to the formation of anti-hydrogen (three body recombination) gives atoms with the weakest binding that can survive the field, the results shown in figure 6 imply that the atoms are more weakly bound than expected.

Acknowledgments

This work was supported by the Chemical Sciences, Geosciences, and Biosciences Division of the Office of Basic Energy Sciences, US Department of Energy, and by the Office of Fusion Energy, US Department of Energy.

References

[1] Gallagher T F 1994 *Rydberg Atoms* (Cambridge: Cambridge University Press)
[2] Vrinceanu D, Granger B E, Parrott R, Sadeghpour H R, Cederbaum L, Mody A, Tan J and Gabrielse G 2004 *Phys. Rev. Lett.* **92** 133402
[3] Choi J-H, Guest J R, Hansis E, Povilus A P and Raithel G 2005 *Phys. Rev. Lett.* **95** 253005
[4] Glinsky M E and O'Neil T M 1991 *Phys. Fluids* B **3** 1279
[5] Andresen G B *et al* (ALPHA Collaboration) 2010 *Nature* **468** 673
[6] Cacciani P, Luc-Koenig E, Pinard J, Thomas C and Liberman S 1988 *J. Phys. B: At. Mol. Opt. Phys.* **21** 3499
[7] Cacciani P, Liberman S, Luc-Koenig E, Pinard J and Thomas C 1989 *Phys. Rev.* A **40** 3026

[8] Cacciani P, Delsart C, Luc-Koenig E and Pinard J 1992 *J. Phys. B: At. Mol. Opt. Phys.* **25** 1991
[9] Seipp I and Taylor K T 1994 *J. Phys. B: At. Mol. Opt. Phys.* **27** 2785
[10] Seipp I, Taylor K T and Schweizer W 1996 *J. Phys. B: At. Mol. Opt. Phys.* **29** 1
[11] Moser I, Mota-Furtado F and O'Mahony P F 1997 *Phys. Rev.* A **55** 3724
[12] Santos J P, Mota-Furtado F, Laranjeira M F and Parente F 1999 *Phys. Rev.* A **59** 1703
[13] Johnson A S and Mota-Furtado F 2001 *Phys. Rev.* A **63** 043412
[14] Wang L, Yang H F, Liu X J, Liu H P, Zhan M S and Delos J B 2010 *Phys. Rev.* A **82** 022514
[15] Farrelly D, Uzer T, Raines P E, Skelton J P and Milligan J A 1992 *Phys. Rev.* A **45** 4738
[16] Fielding H H, Wals J, van der Zande W J and van Linden van den Heuvell H B 1995 *Phys. Rev.* A **51** 611
[17] Salas J P and Lanchares V 1998 *Phys. Rev.* A **58** 434
[18] Ihra W, Mota-Furtado F and O'Mahony P F 1998 *Phys. Rev.* A **58** 3884
[19] Courtney M 1995 *Phys. Rev.* A **51** 4558
[20] Iken M A, Borondo F, Benito R M and Uzer T 1994 *Phys. Rev.* A **49** 2734
[21] Owen S M, Monteiro T S and Dando P A 2000 *Phys. Rev.* E **62** 6388
[22] Bass E M and Dubin D H E 2009 *Phys. Plasmas* **16** 012101
[23] Press W H, Teukolsky S A, Vetterling W T and Flannery B P 1992 *Numerical Recipes* 2nd edn (New York: Cambridge University Press)
[24] Topcu T and Robicheaux F 2007 *J. Phys. B: At. Mol. Opt. Phys.* **40** 1925
[25] Robicheaux F 1996 *J. Phys. B: At. Mol. Opt. Phys.* **29** 779